Korean J. Chem. Eng., 40(7), 1709-1714 (2023)
DOI: 10.1007/s11814-023-1396-0

pISSN: 0256-1115
eISSN: 1975-7220

Utilization of functionalized silane coatings for enhanced mechanical properties of hydroxyapatite filler

Eunhyun Ji*,‡, Young Hoon Song,‡, Jeong Hyun Seo**,†, and Kye Il Joo*,†**

*Division of Chemical Engineering and Materials Science, Ewha Womans University, Seoul 03760, Korea
**School of Chemical Engineering, Yeungnam University, 280 Daehakro, Gyeongsan, Gyeongbuk 38541, Korea
(*Received 27 December 2022 • Revised 28 January 2023 • Accepted 31 January 2023*)

Abstract−Silane coupling agents are widely used as molecular bridges between inorganic minerals and organic materials to modify surface properties for diverse biomedical applications. In this study, we developed hydroxyapatite (HAp)-based scaffolds by fabricating the surface of HAp pellets with silane coupling agents containing methacrylate, amine, and carboxylic acid functional groups to improve their mechanical properties for use as biodegradable fillers in dental and bone regeneration applications. Surface coating with carboxylic acid-functionalized silane exhibited a substantially enhanced mechanical strength of up to 30 MPa, which possibly resulted from the stable configuration of interfacial bonding via electrostatic attractive interaction in the a-planes of the HAp pellets. Furthermore, the functionalized silane-coated HAp scaffolds displayed excellent biocompatibility, which suggests that they could be utilized as bone filler composites for bone tissue engineering.

Keywords: Hydroxyapatite, Silane Coupling, Molecular Bridge, Agglomeration, Surface Modification

INTRODUCTION

Calcium phosphate-based bioceramics are commonly used in dental and orthopedic reconstruction because of their excellent biocompatibility, bioactivity, and osteoconductivity [1-3]. Among several bioceramics, hydroxyapatite (HAp) is mainly found in bone and teeth minerals and therefore has been considered an excellent candidate for bone graft and regeneration [4-6]. Furthermore, HAp has been used as a biodegradable filler in dental resin composites because it possesses physicochemical properties similar to those of human dental tissues. It is also viscoelastic and highly resistant to moisture [7,8]. Several attempts have been made to develop HAp composite materials with synthetic or natural polymers, including polycaprolactone (PCL), polymethylmethacrylate (PMMA), poly(lactic-co-glycolic acid) (PLGA), and collagen, to improve the mechanical strength and bioactivity of HAp fillers in bone and dental applications [9-13]. In particular, interfacial bonding between the polymeric matrix and inorganic HAp filler is a pivotal factor that determines the mechanical and physicochemical properties of HAp composites. Therefore, several studies have proposed to modify the surface properties of HAp using coupling agents to enhance the interfacial compatibility of HAp composite scaffold [14-17].

Silanes are coupling agents containing functional groups capable of bonding with both organic and inorganic materials. They are widely used as molecular bridges between organic polymers and inorganic minerals to improve mechanical strength and modify surface properties [18,19]. Recent studies have reported that silane coatings on the surfaces of biomaterial scaffolds can enhance interfacial adhesion, bioactivity, cell adhesion, and protein immobilization [20-24]. Thus, silane has been widely utilized in biomaterial engineering applications, including bone grafts, dental implants, and biosensors.

In this study, we developed HAp scaffolds coated with silane coupling reagents containing methacrylate, amine, and carboxylic acid functional groups to improve the mechanical properties of HAp through increasing the interfacial interactions between HAp pellets. The results demonstrated that the functionalized silane-coated HAp pellets exhibited substantially enhanced mechanical strength of the scaffold with no obvious signs of cellular toxicity; thereby, they could be potential bone filler composites for bone regeneration and tissue engineering.

MATERIALS AND METHODS

1. Materials

3-Methacryloxypropyltrimethoxysilane (3MPS) and 3-aminopropyltrimethoxysilane (APTMS) were purchased from Sigma-Aldrich (St. Louis, MO, USA). Carboxyethylsilanetriol sodium salt (CES) was obtained from Biosynth Carbosynth Ltd. (Staad, Switzerland). HAp pellets were purchased from Sigma-Aldrich and used without further purification.

To prepare sintered HAp (sHAp) pellets, HAp pellets were poured into a 20-mm diameter cylindrical mold and pressed at 10 MPa for 5 s. The resultant HAp disks were then sintered at atmospheric pressure at 1,200 °C for 1 h in an electric tube furnace (Ajeon Heating Industrial Co. Ltd., Seoul, Korea). Next, sHAp pellets were prepared through pulverizing the sHAp disks with a motor and then

†To whom correspondence should be addressed.
E-mail: jhseo78@yu.ac.kr, kijoo@ewha.ac.kr
‡These authors contributed equally to this work.

collecting them using a 200 μm standard test sieve. Our previous study showed a uniform size distribution of sHAp pellets with no agglomerates larger than 4 μm [6].

2. Fabrication of the Functionalized Silane-coated HAp and sHAp Scaffolds

The silane coupling agents, 3MPS, APTMS, and CES, were pre-activated in 1 mM of HCl for 30 min and then mixed with HAp or sHAp pellets in distilled water for 1 min. The mixture was poured into a cylindrical mold (7 mm diameter×25 mm height) and then compressed using a manual hydraulic press (J-1, Asone, Osaka, Japan) at 60 MPa for 30 s to form silane-coated HAp or sHAp scaffolds. The HAp and sHAP scaffolds were then removed from the mold and dried at 60 °C for 1 d before further analysis.

3. Compressive Strength of the Functionalized Silane-coated HAp and sHAp Scaffolds

The compressive strengths of the non- and silane-coated HAp and sHAp scaffolds were directly measured using the Instron universal testing machine (Instron, Norwood, MA, USA) with a 5,000 N load cell. The sample scaffolds were horizontally placed in the compression test fixture, and a load was applied at a constant rate of 10 mm/min. Each measurement was repeated at least five times and the average for a given sample was determined.

4. Fourier-transform Infrared (FTIR) Spectroscopy Analysis

FTIR spectra of non- and silane-coated HAp and sHAp scaffolds were obtained using the Spectrum 100 FTIR spectrometer (PerkinElmer, Waltham, MA, USA) over a scan range of 600-4,000 cm^{-1} at an operating spectral resolution of 1.0 cm^{-1}.

5. Scanning Electron Microscope (SEM) and Energy Dispersive X-ray Spectrometry (EDX) Analysis

For the surface morphological analysis of non- and silane-coated HAp and sHAp scaffolds, the sample scaffolds were mounted on the conductive carbon sheet of an SEM specimen holder, sputter-coated using the E-1030 coater (Hitachi, Tokyo, Japan) equipped with a platinum target and then viewed using the S-4200 SEM (Hitachi).

EDX analysis was performed using the EMAX spectrometer (Horiba, Kyoto, Japan) to analyze the elemental composition of the functionalized silane-coated scaffolds.

6. *In vitro* Cell Viability Assay

The *in vitro* cell viability of non- and silane-coated HAp and sHAp scaffold was quantitatively determined using the Cell Counting Kit-8 (CCK-8, Dojindo, Japan) with NIH-3T3 cells maintained in a 5% CO_2 environment in Dulbecco's modified Eagle's medium (DMEM; Hyclone, Logan, UT, USA) supplemented with 10% (v/v) fetal bovine serum (Hyclone) and 1% (v/v) streptomycin (Hyclone). Following the ISO 10993-5 *in vitro* cell viability evaluation, the sample scaffold extracts were prepared through incubating the scaffold in a cell culture medium at 37 °C for 24 h. Cells were seeded overnight in a 96-well culture plate, and the medium was replaced with a culture medium containing 5 mg/mL of sample scaffold extracts. Cell viability was determined after 72 h of culture via the CCK-8 assay, and the results were normalized against those of cells maintained in a blank culture medium. Each measurement was repeated at least three times and the average for a given sample was determined. Live-dead cells were imaged using a live/dead

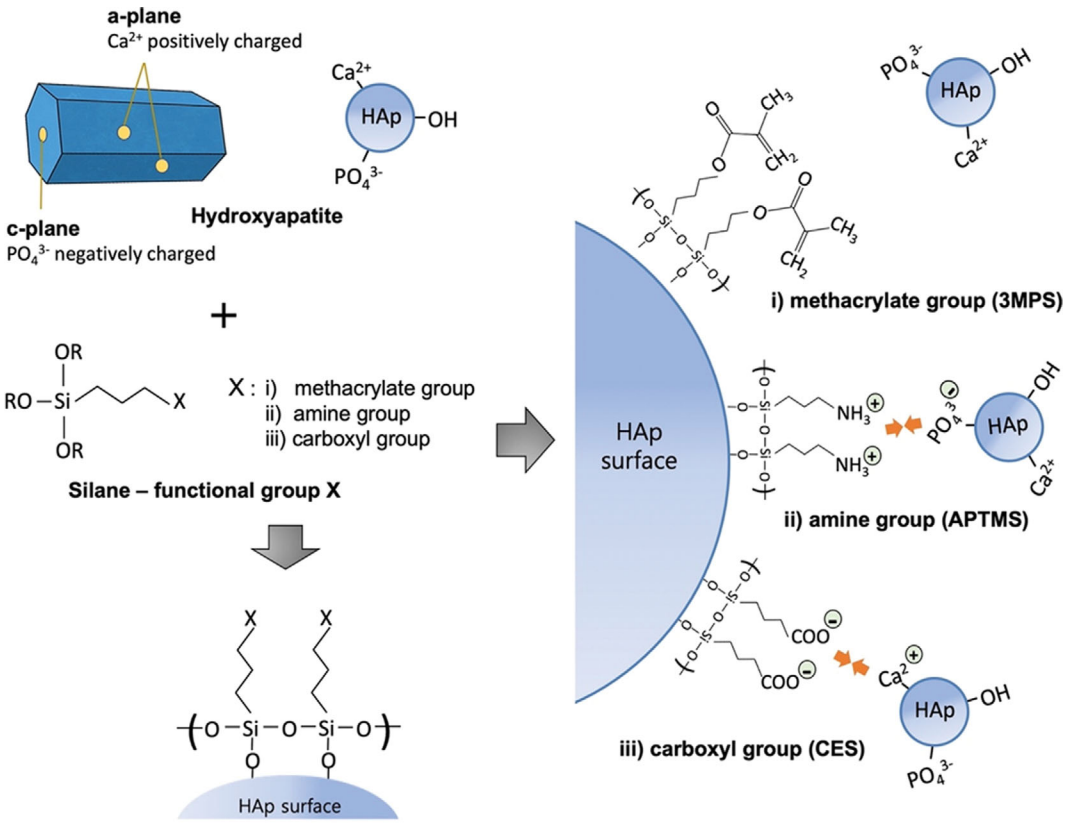

Fig. 1. Schematic illustration of the fabrication of functionalized silane-coated HAp scaffolds.

viability/cytotoxicity kit (Invitrogen, Waltham, MA, USA) and a fluorescence microscope (BX60; Olympus, Tokyo, Japan).

RESULTS AND DISCUSSION

1. Fabrication of the Functionalized Silane-coated HAp and sHAp Scaffolds

To prepare the functionalized silane-coated HAp pellets, silane coupling reagents containing methacrylate (3MPS), amine (APTMS), and carboxylic acid (CES) functional groups were activated in 1 mM HCl for 30 min. The HAp pellets were then incubated with the activated silane coupling agents for 1 min. The resultant HAp pellets were placed into a cylindrical mold and compressed to fabricate functionalized silane-coated HAp scaffolds designated as HAp-3MPS, HAp-APTMS, and HAp-CES (Fig. 1). The sHAp pellets were prepared through the conventional sintering process, which is widely employed to improve the mechanical strength of HAp by increasing its densification. To prepare functionalized silane-coated sHAp scaffolds, sHAp pellets were incubated with silane coupling reagents, 3MPS, APTMS, and CES, and the resultant sHAp pellets were then placed into the mold and compressed to fabricate sHAp scaffolds designated as sHAp-3MPS, sHAp-APTMS, and sHAp-CES, respectively.

2. Mechanical Properties of the Functionalized Silane-coated HAp and sHAp Scaffolds

HAp has a hexagonal rod-like shape elongated along the c-axis, and the corresponding a- and c-planes differ in their orientation and ion compositions [25-27]. The a-planes are rich in calcium ions (Ca^{2+}), which leads to a positively charged surface, whereas the c-planes are negatively charged, as they are rich in phosphorus (PO_4^{3-}) and hydroxide (OH^-) ions [28-30]. Furthermore, the agglomeration of HAp pellets is mainly initiated by the electrostatic attractive interactions between the oppositely charged Hap surfaces. Therefore, the configuration of the interfacial interaction between HAp pellets during agglomeration significantly affects the mechanical properties of HAp scaffolds.

To examine the mechanical properties of the functionalized silane-coated scaffolds, the stress-strain curve was obtained for the scaffolds using an Instron universal testing machine (Fig. 2(a)), and Young's modulus and compressive strength of the scaffolds were determined (Fig. 2(b) to 2(d)). The result indicated that the compressive strength of the noncoated HAp scaffold was approximately 19.3 MPa, whereas the HAp-3MPS scaffold exhibited slightly lower mechanical strength, which implies that the surface coating of HAp pellets with methacrylate-functionalized silanes possibly caused the reduced charge attraction between HAp pellets (Fig. 2(c)). Similarly, no notable changes were observed in the compressive strength of the HAp-APTMS scaffold, which suggests that the surface coating of HAp pellets with amine groups did not significantly improve the electrostatic attractive interaction between HAp pellets. However, the HAp-CES scaffold exhibited a gradual increase in compressive strength of up to 30.8 MPa as the concentration of the silane

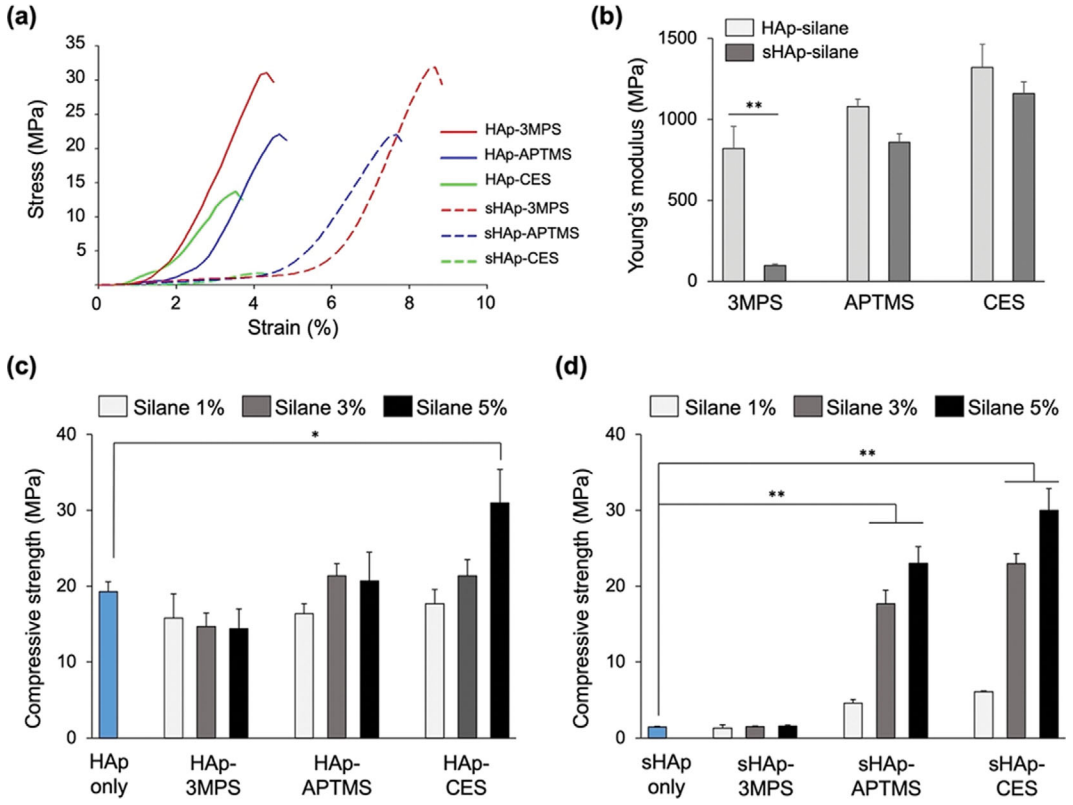

Fig. 2. Mechanical properties of the functionalized silane-coated scaffolds. (a) Stress-strain curve of the silane-coated HAp and sHAp scaffolds. Evaluation of Young's modulus (b) and compressive strength of functionalized silane-coated HAp (c) and sHAp (d) (n≥5). Error bars represent the standard error of the mean; *p<0.05; **p<0.01.

coupling reagent with CES increased. The substantially enhanced mechanical strength of the HAp-CES scaffold can be attributed to the increased interfacial bonding between the negatively charged surface in the a-planes of the CES-coated HAp pellet and the positively charged surface in the a-planes of the Ca^{2+}-rich HAp pellet, which is a relatively stable configuration for the agglomeration of HAp pellets.

The noncoated sHAp scaffold exhibited significantly reduced compressive strength, which was possibly due to the hydrophobic features of the sHAp obtained after the sintering process, resulting in weak interfacial bonding strength between the sHAp pellets in hydrophilic environments (Fig. 2(d)). The surface coating of sHAp with 3MPS did not affect its mechanical properties, whereas improved compressive properties were observed in the sHAp-APTMS scaffold as the concentration of silane coupling reagents increased. Furthermore, the sHAp scaffold coated with CES exhibited remarkably enhanced mechanical strength of up to 30 MPa. These results suggest that surface coating of HAp and sHAp pellets with CES significantly improves the compressive strength of the scaffolds owing to the increased interfacial bonding between the pellets.

3. Characterization of the Functionalized Silane-coated sHAp Scaffolds

The functionalized silane-coated scaffolds were further characterized via FTIR spectroscopy. FTIR spectra of noncoated HAp and sHAp and silane-coated sHAp scaffolds were obtained over a scan range of 600-4,000 cm^{-1} at an operating spectral resolution of 1.0 cm^{-1} (Fig. 3). FTIR analysis of the HAp scaffold showed characteristic peaks of PO_4^{3-} at 562 cm^{-1}, 601 cm^{-1}, and 1,000-1,100 cm^{-1} and the O-H vibration modes at 634 cm^{-1} and 3,430 cm^{-1}, whereas the weak adsorbed water bands were observed at 1,628 cm^{-1} and 634 cm^{-1} and disappeared in the sHAp scaffold. The functionalized silane coating resulted in the characteristic peaks of the carbonyl, N-H, and carboxylate group stretching vibrations at 1,720 cm^{-1} for the sHAp-3MPS, 1,637 cm^{-1} for sHAp-APTMS, and 1,568 cm^{-1} for sHAp-CES scaffolds, respectively. These results confirmed that surface modification with functionalized silane could properly introduce functional groups to the sHAp pellets and scaffolds.

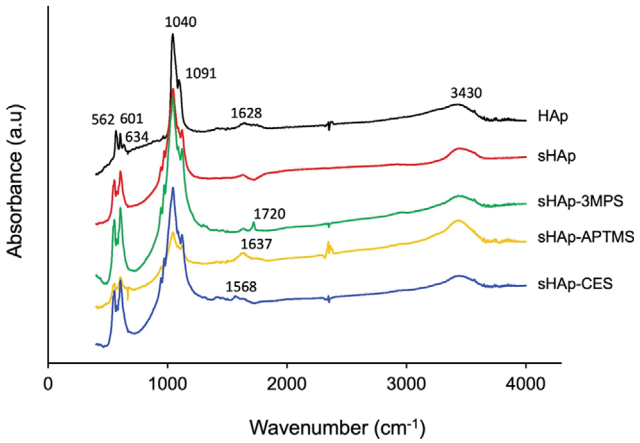

Fig. 3. Fourier-transform infrared spectroscopy (FTIR) analysis of noncoated HAp and sHAp and functionalized silane-coated sHAp scaffolds.

To further assess the surface modification of the scaffolds with functionalized silane, the elemental composition of the scaffolds was analyzed via EDX spectrometry. The EDX spectra of the sHAp-APTMS scaffold showed the characteristic peaks of Si and C, whereas those of the sHAp-CES scaffold showed the characteristic peaks of Si, Na, and C, which imply the presence of a function-

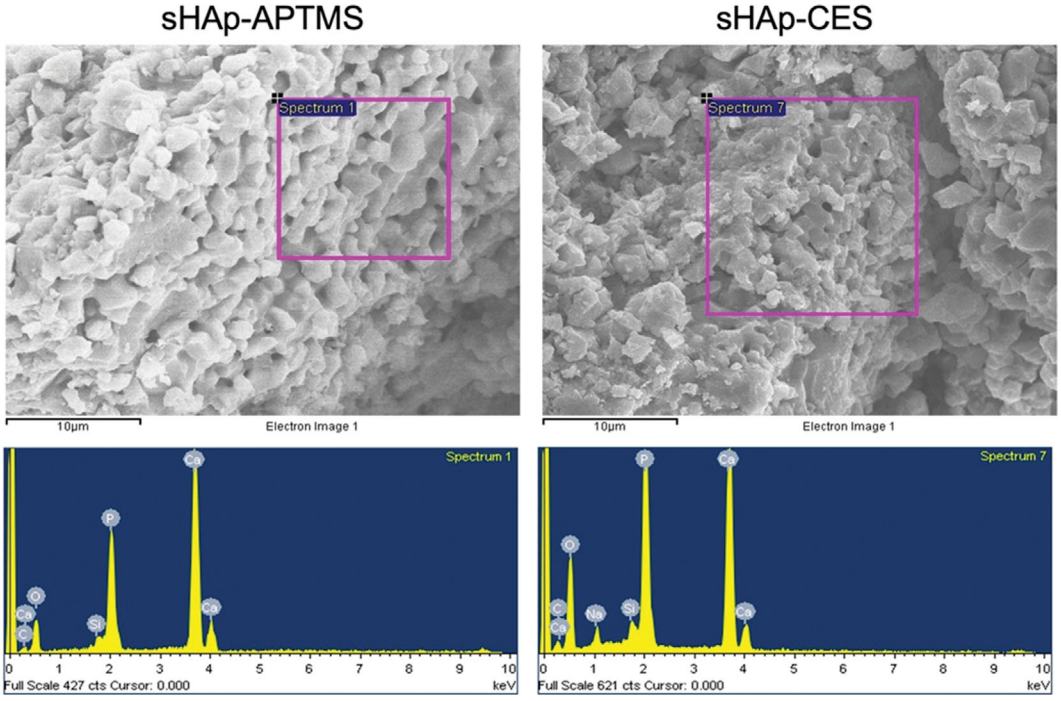

Fig. 4. Energy dispersive X-ray spectrometry (EDX) of sHAp-APTMS and sHAp-CES scaffolds.

alized silane coating on the scaffold surface (Fig. 4).

In addition, the surface morphology and densification of the scaffolds were examined using SEM. Morphological analysis of noncoated HAp and sHAp scaffolds showed that the relative surface densification decreased in the sHAp scaffold, owing to the reduced particle agglomeration of hydrophobic sHAp pellets (Fig. 5, top). Silane coating of sHAp with 3MPS had a minimal effect on the surface morphology, whereas coating with APTMS and CES substantially increased the interfacial bonding between the sHAp pellets, which resulted in dense structures at the surface of the scaffolds (Fig. 5, bottom). Overall, these results indicate that silane coating with CES could remarkably improve the mechanical properties of sHAp scaffolds through enhancing intermolecular interactions between sHAp pellets.

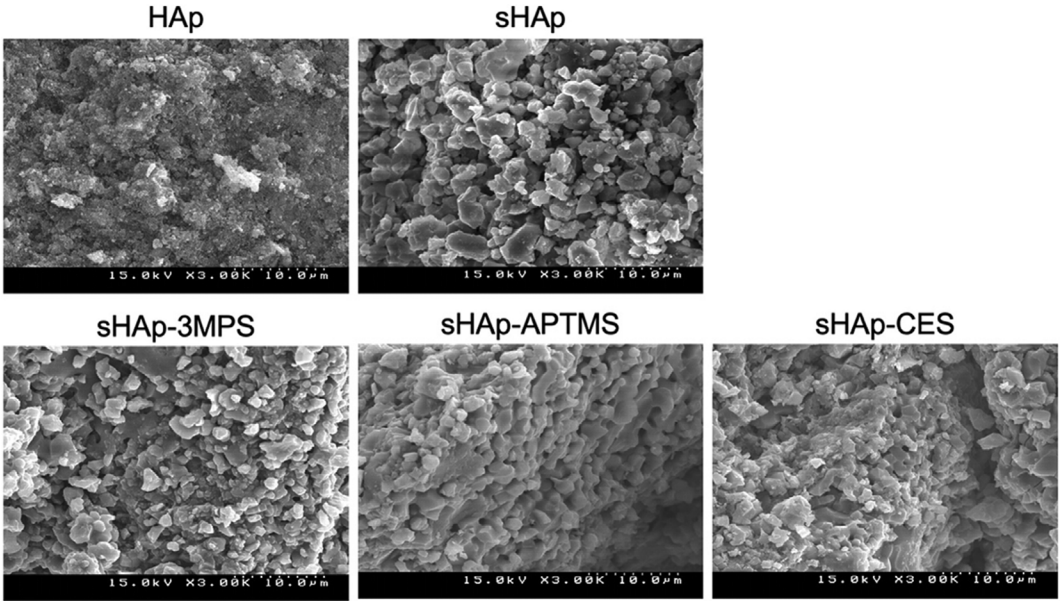

Fig. 5. Scanning electron microscopy images of the surface of noncoated HAp and sHAp and functionalized silane-coated sHAp scaffolds.

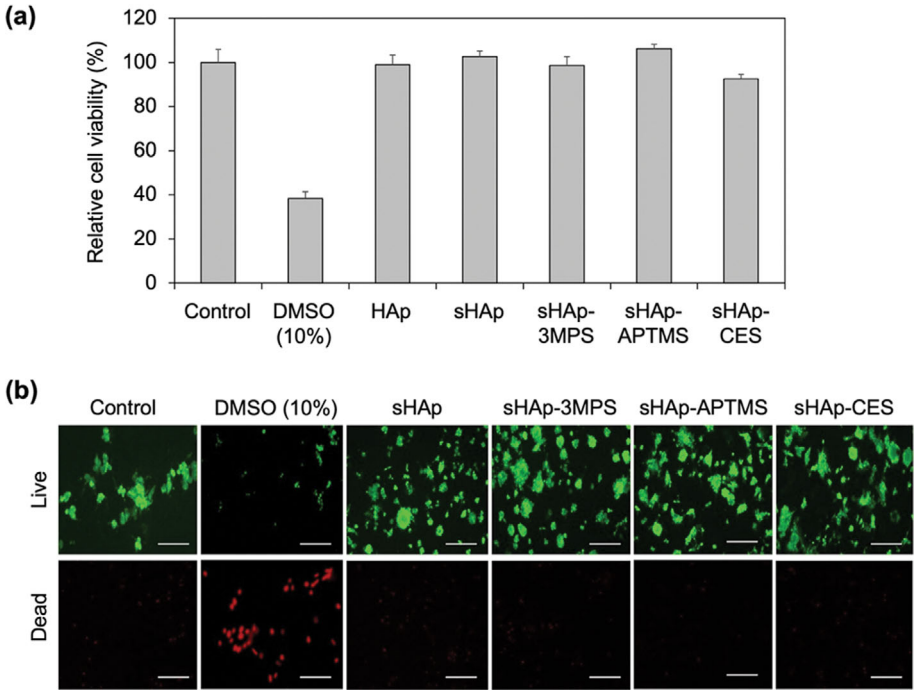

Fig. 6. Effects of functionalized silane-coated sHAp scaffolds on cell viability. The cell viability of noncoated HAp and sHAp and functionalized silane-coated sHAp scaffolds based on the CCK-8 assay results after 72 h incubation of NIH-3T3 cells with the corresponding scaffold extracts (a) (n≥3) and live-dead fluorescent images (b) (scale bar, 200 μm).

4. Effects of Functionalized Silane-coated sHAp Scaffolds on Cell Viability

To further evaluate the cell viability of the noncoated HAp and sHAp and silane-coated sHAp scaffolds, cell viability was quantitatively assessed via the CCK-8 assay in mouse fibroblast NIH-3T3 cells. To prepare scaffold extracts, the scaffolds were incubated in a cell culture medium at 37 °C for 24 h. Next, NIH-3T3 cells seeded in the culture plate overnight were cultured for 72 h in the culture medium containing 5 mg/mL of the scaffold extract. The cell viability was then measured using the CCK-8 assay kit and compared with positive and negative controls. The results show that more than 95% of the cells were viable compared with cells cultured in a blank culture medium, which indicates the absence of notable cytotoxic effect on the silane-coated sHAp scaffolds (Fig. 6(a)). The results were further confirmed by visualizing viable cells in calcein-acetoxymethyl-based live-dead assay (Fig. 6(b)), thereby demonstrating the excellent biocompatibility of the functionalized silane-coated sHAp scaffolds.

CONCLUSION

We fabricated HAp-based scaffolds coated with a silane containing methacrylate (3MPS), amine (APTMS), and carboxylic acid (CES) functional groups and compared their mechanical properties and cytocompatibilities. Surface coating of HAp and sHAp with CES-functionalized silane exhibited substantially improved mechanical strength, which could be attributed to increased interfacial bonding via electrostatic attractive interaction in the a-planes of the pellets. These results suggest that the stable configuration for particle agglomeration provides mechanical support to the scaffold. Furthermore, the functionalized silane-coated sHAp scaffolds showed excellent biocompatibility, thereby showing great potential as bone filler composites for bone regeneration applications.

ACKNOWLEDGEMENTS

This work was supported by the 2019 Yeungnam University Research Grant.

REFERENCES

1. N. Eliaz and N. Metoki, *Materials*, **10**, 334 (2017).
2. R. A. Surmenev, M. A. Surmeneva and A. A. Ivanova, *Acta Biomaterialia*, **10**, 557 (2014).
3. S. V. Dorozhkin, *Biomaterials*, **31**, 1465 (2010).
4. P. P. Patel, C. Buckley, B. L. Taylor, C. C. Sahyoun, S. D. Patel, A. J. Mont, L. Mai, S. Patel and J. W. Freeman, *J. Biomed. Mater. Res. Part A*, **107**, 732 (2019).
5. J. Jeong, J. H. Kim, J. H. Shim, N. S. Hwang and C. Y. Heo, *Biomater. Res.*, **23**, 4 (2019).
6. Y. Song, K. I. Joo and J. H. Seo, *Biotechnol. Bioprocess Eng.*, **26**, 201 (2021).
7. K. Akhtar, C. Pervez, N. Zubair and H. Khalid, *J. Mater. Sci.: Mater. Med.*, **32**, 129 (2021).
8. C. Santos, Z. B. Luklinska, R. L. Clarke and K. W. M. Davy, *J. Mater. Sci.: Mater. Med.*, **12**, 565 (2001).
9. J. Venkatesan and S. Anil, *Biotechnol. Bioprocess Eng.*, **26**, 312 (2021).
10. D. Puppi, F. Chiellini, A. M. Piras and E. Chiellini, *Prog. Polym. Sci.*, **35**, 403 (2010).
11. K. Rezwan, Q. Z. Chen, J. J. Blaker and A. R. Boccaccini, *Biomaterials*, **27**, 3413 (2006).
12. Z. Wang, S. Wang, Y. Marois, R. Guidoin and Z. Zhang, *Biomaterials*, **26**, 7387 (2005).
13. E.-j. Cheon, S.-H. Kim, D.-K. Lee, Y.-K. Jo, M.-R. Ki, C.-J. Park, H.-S. Jang, J.-S. Ahn, S.-P. Pack and S.-H. Jun, *Biotechnol. Bioprocess Eng.*, **26**, 923 (2021).
14. R. A. Sousa, R. L. Reis, A. M. Cunha and M. J. Bevis, *J. Mater. Sci. Mater. Med.*, **14**, 475 (2003).
15. Z. Fang and Q. Feng, *Mater. Sci. Eng. C*, **35**, 190 (2014).
16. O. G. Cisneros-Pineda, W. Herrera Kao, M. I. Loría-Bastarrachea, Y. Veranes-Pantoja, J. V. Cauich-Rodríguez and J. M. Cervantes-Uc, *Mater. Sci. Eng. C*, **40**, 157 (2014).
17. F. Liu, B. Sun, X. Jiang, S. S. Aldeyab, Q. Zhang and M. Zhu, *Dent. Mater.*, **30**, 1358 (2014).
18. Y. Xie, C. A. S. Hill, Z. Xiao, H. Militz and C. Mai, *Compos. Part A: Appl. Sci. Manuf.*, **41**, 806 (2010).
19. S. C. Chowdhury, R. Prosser, T. W. Sirk, R. M. Elder and J. W. Gillespie, *Appl. Surf. Sci.*, **542**, 148738 (2021).
20. C. Shuai, C. Shuai, P. Feng, Y. Yang, Y. Xu, T. Qin, S. Yang, C. Gao and S. Peng, *Molecules*, **22**, 511 (2017).
21. F. Ghorbani, M. Pourhaghgouy, T. Mohammadi-hafshehjani and A. Zamanian, *Silicon*, **12**, 3015 (2020).
22. A. Nikbakht, C. Dehghanian and R. Parichehr, *RSC Adv.*, **11**, 26127 (2021).
23. Y. J. Chuah, S. Kuddannaya, M. H. A. Lee, Y. Zhang and Y. Kang, *Biomater. Sci.*, **3**, 383 (2015).
24. S. Somasundaram, *J. Biomed. Mater. Res. B Appl. Biomater.*, **106**, 2901 (2018).
25. R. Astala and M. J. Stott, *Phy. Rev. B*, **78**, 075427 (2008).
26. H. Oonishi, *Biomaterials*, **12**, 171 (1991).
27. W. Suchanek and M. Yoshimura, *J. Mater. Res.*, **13**, 94 (1998).
28. I. S. Harding, N. Rashid and K. A. Hing, *Biomaterials*, **26**, 6818 (2005).
29. Z. Zhuang, T. J. Fujimi, M. Nakamura, T. Konishi, H. Yoshimura and M. Aizawa, *Acta Biomater.*, **9**, 6732 (2013).
30. Y. In, U. Amornkitbamrung, M.-H. Hong and H. Shin, *ACS Omega*, **5**, 27204 (2020).